Progress In Electromagnetics Research M, Vol. 97, 177–188, 2020

Flexible Vivaldi Antenna Based on a Fractal Design for RF-Energy Harvesting

Mustafa A. Al-Janabi* **and Sema K. Kayhan**

Abstract—Radio frequency (RF) energy harvesting technologies have attracted different efforts from researchers to employ low energy in powering portable electronic devices. In this article, an Ultra-Wide Band (UWB) antenna based on a Vivaldi fractal antenna backed with a Metamaterial (MTM) array is exemplified for RF-energy harvesting in the modern 5G networks. The antenna is connected to a full wave rectifier circuit to obtain a rectified DC current. It is found that the exemplified antenna provides a maximum output voltage of 1.4 V and 1.3 V at 3.1 GHz and 4 GHz, respectively, when the incident RF power is around 17 Bm. The measured results and simulations show excellent agreement. The antenna is printed on a flexible Kodak photo paper of 0.5 mm thickness with $\varepsilon_r = 2$ and loss tangent of 0.0015. The numerical simulations are conducted using CST MWS software package. The proposed antenna structure is fabricated using an ink jet printing technology based on conductive silver nanoparticle ink. Finally, from the obtained measurements after the comparison to their simulations, the proposed antenna covers the frequency band from 2.4 GHz up to 20 GHz with a gain of 1.8 dBi at 3.1 GHz and 4 dBi at 4 GHz.

1. INTRODUCTION

Since the concept of metamaterial (MTM) structures was started from the optical domain in 1987 [1] as photonic band gap, they have received a lot of research attention. As of late, an intensive investigation has been applied to the effects on connecting the MTM structures to antenna performance for upgrading their performance [1]. MTM structures are periodic-like layers of exceptional surface wave concealment properties with unique constitutive electromagnetic parameters, permittivity, and permeability, which are not found in nature [2]. Based on their nontraditional electromagnetic properties, MTM structures were classified as: near zero refractive index [3], soft and hard surfaces [4], high-impedance surfaces [5], and artificial magnetic conductors [6]. It is worth to say that a few of these structures have relatively enhanced electromagnetic properties with low material losses [7].

Frequency Selective Surface (FSS) is another category of MTM structures that are periodically layered as dielectric and/or metallic unit cells in different manners [8] with high frequency selectivity. Recently, FSS classifications are defined according to their applications whether as filters [9], artificial magnetic conductors [10], photonic crystals [11], and photonic band gaps [12]. These structures can also be as artificial periodic and non-periodic layers to prevent and/or assist the incident wave propagation [13]. They possess high impedance in both TE and TM modes as found in mushroom-like structures [14], in which an in-phase reflection coefficient can be created [15]. Moreover, soft and hard surfaces operate as FSS structures [16], which include a wide range of applications in the antenna engineering researches and industries.

Received 30 July 2020, Accepted 10 October 2020, Scheduled 20 October 2020
* Corresponding author: Mustafa A. Al-Janabi (mustafa.aljanabi@gantep.edu.tr).
The authors are with the Electrical and Electronics Department, Gaziantep University, Gaziantep, Turkey.

2. ECFCPW TRANSMISSION LINE DESIGN AND DISCUSSIONS

The most fundamental challenge in any antenna design is the matching impedance bandwidth especially for miniaturized antenna profiles [21]. Therefore, a great impact of research targeting UWB radiators between 3.1 GHz and 10 GHz, $|S_{11}| < -10$ dB, with an acceptable gain over 2 dBi, for medium and long range of communication distances was targeted. One of the most important features to achieve UWB matching impedance is the feeding structure. Therefore, in this section a novel study based on analytical and numerical simulations to design an exponential curved flared coplanar waveguide (ECFCPW) transmission line is proposed. The ECFCPW structure is etched from a copper layer with an input reflection coefficient (Γ_{in}) given by a fundamental equation [2]:

$$\Gamma_{in} = \text{sinc}\,(\beta l) \tag{1}$$

where β is the phase constant, and l is the transmission line length. The reflection coefficient at the source (Γ_o) at any length can be calculated by [2]:

$$\Gamma_o = 0.5 \ln z_n e^{j\beta l} \Gamma_{in} \tag{2}$$

where z_n is the normalized impedance coefficient. For the proposed antenna, the conducted ECFCPW dimensions are structured to follow an exponential curve given by:

$$y_1 = a_1 e^{x_1 L_1} \tag{3}$$

$$y_2 = a_2 e^{x_2 L_2} \tag{4}$$

where $x_1 = 0.12$ is the exponential factor for the microstrip line, and $x_2 = 0.18$ is the exponential factor for the ground plane. L_1 is the microstrip line length, and L_2 is the ground plane length. The factors a_1 and a_2 are curve factors 2 and 3, respectively. It is important to mention that Equations (3) and (4) factors are computed from parametric study as will be seen later.

Now, the proposed ECFCPW performance in terms of S-parameters is evaluated using CST MWS [25]. The magnitudes of S_{11} and S_{12} spectra are presented in Fig. 1(a). It is found that

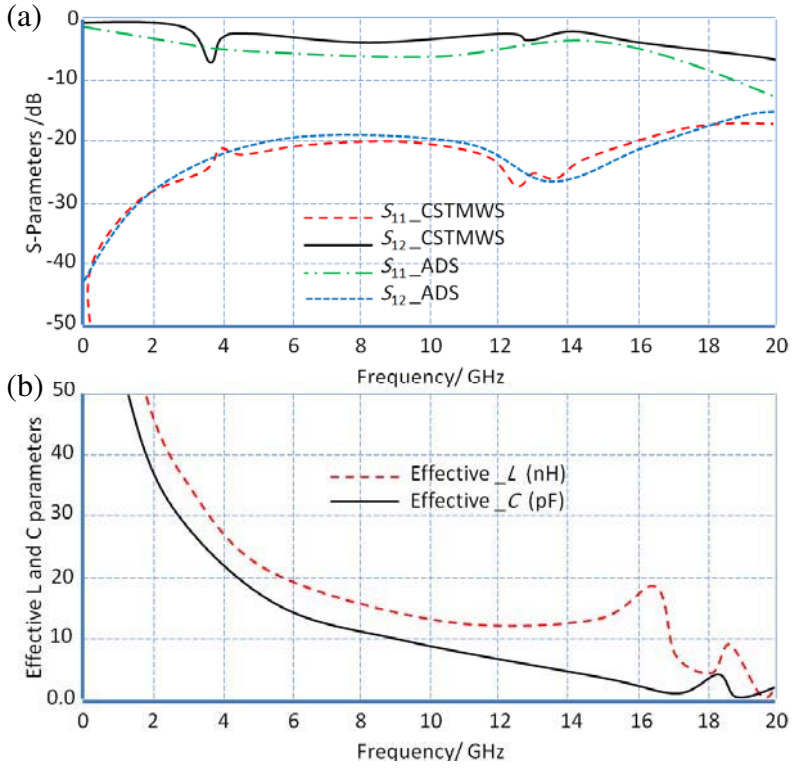

Figure 1. L and C parameters of the proposed ECFCPW transmission line.

the proposed transmission line provides an excellent matching over a wide bandwidth, in which S_{11} magnitude is found less than $-10\,\text{dB}$ over all frequencies of interest. ADS simulation based circuit analysis is invoked to validate the obtained numerical results from CSTMWS for the proposed ECFCPW structure. The effective inductive (L) and capacitive (C) variations of the proposed ECFCPW structure are evaluated using the method proposed in [7] as presented in Fig. 1(b). This variation leads the authors to a decision that using such a transmission line in the rectenna design could be possible without the need of using extra inductor and/or capacitor elements as will be seen later.

It is worth to mention that the values of L and C parameters of the proposed ECFCPW at $Z_0 = 50\,\Omega$ are calculated according to the following equation:

$$L = \frac{Z_0}{S_{12}}\left[\frac{1-(\omega/\omega_r)^2}{\omega}\right] \tag{5}$$

$$C = \left[1-\left(\frac{\omega}{\omega_r}\right)^2\right]\frac{S_{12}}{\omega Z_0} \tag{6}$$

where ω is the frequency, and ω_r is the frequency resonance to be out of the band of interest [19]. Moreover, the authors consider the losses that are relative in such a transmission line from the following equation:

$$R = 2Z_0\left[\frac{1}{2S_{12}} - 1\right] \tag{7}$$

3. MTM STRUCTURE PERFORMANCE

In this section, the proposed MTM structure performance is tested analytically and numerically. For this, the constitutive electromagnetic parameters are investigated through characterizing the propagation constant, reflection phase, and dispersion spectra based on the proposed approach in [20]. The proposed MTM is constructed from a 5×6 square metal pad array mounted on the back panel of the substrate which creates 4×5 slots as seen in Figure 2. The individual MTM unit cell periodical dimensions are given by (p) of $3.6\,\text{mm} \times 3.6\,\text{mm}$ and spaced with a gap (g) of $0.4\,\text{mm}$.

Now, such an array may create a capacitive behavior (C_{MTM}) given by Equation (8) [16]. Therefore, the attributed behavior exhibits a low pass filter [22]. Nonetheless, unbalanced circuit is the result of such an array due to the inductive component absence, which indicates a significant influence on surface current motion along the MTM width in comparison to the MTM length [23].

$$C_{\text{MTM}} = \frac{p\varepsilon_0\,(1+\varepsilon_r)}{\pi}\cosh^{-1}\left(\frac{p+g}{g}\right) \tag{8}$$

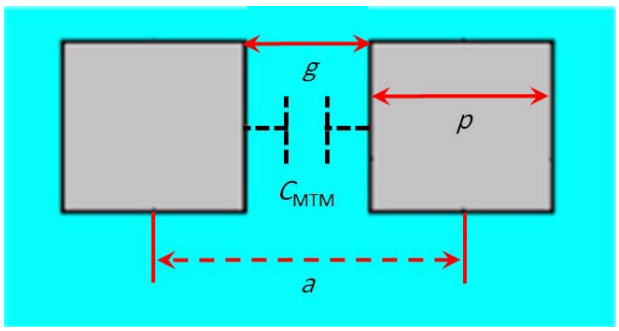

Figure 2. The proposed MTM structure equivalent capacitor.

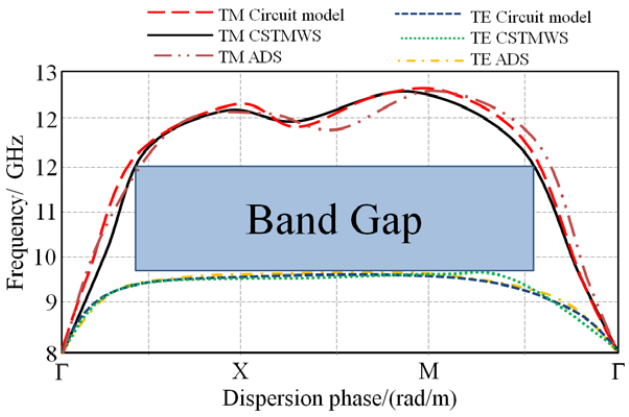

Figure 3. Dispersion diagram.

The MTM performance is mainly affected by the number of slots ($m \times n$); for this, $m < n$ to realize high capacitive reactance along the antenna width for suppressing the surface waves [24]. To validate this hypothesis, the dispersion diagram and reflection phase spectra from CSTMWS and ADS software packages are realized. In the simulation, the band-gap, natural resonances, and dispersion properties are localized for the proposed MTM. In these calculations, the propagation constant (γ) for the proposed unit cell is computed at the First Brillion Zone (FBZ) for TE and TM modes [17] in the crystal lattice (Γ, χ, M) vertex as seen in Figure 3.

From the resulting dispersion diagram, see Figure 3, it is found that the propagation between 8 GHz and 12 GHz is prohibited. The obtained results in Figure 3 are validated analytically based on circuit model. Nonetheless, the ADS simulation is carried out to characterize the reflection phase characteristics and compared to the CSTMWS results for the MTM structure. Based on circuit model and ADS simulations, see Figure 4(a), as sub-networks within a single design, it is found that the unit cell shows reflection phase behavior between 8 GHz and 12 GHz. After that, the electromagnetic properties in terms of ε_r and μ_r for the proposed unit cell are evaluated and presented in Figure 4(b) with and without a substrate. It is found that the introduction of the substrate layer has a significant effect on the retrieved ε_r and μ_r due to the change of the guided wavelength [10].

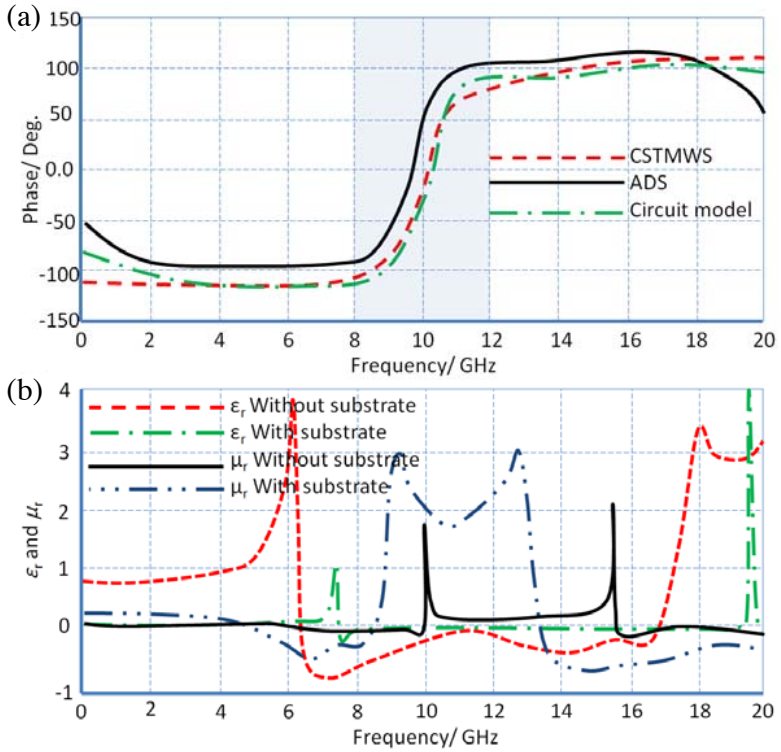

Figure 4. Unit cell characteristics including; (a) Reflection phase and (b) relative electromagnetic properties.

To realize the effects of MTM unit cell dimensions on the capacitance change, the authors apply an analytical study to realize the best MTM dimensions with different available commercial substrates. In this study, the substrate thickness is fixed to 0.5 mm to achieve easy bending and antenna structure embedding. Nevertheless, the used substrates in this study as numerical models are Kodak photo paper, Rogers RO 3006, Polyimide, and FR4. The evaluated reactance values are presented in Figure 5(a) with different values of the relative permittivity considered in this study. It is found that the capacitance significantly increases with increasing p/g. Nevertheless, the influence of changing the permittivity value is observed through the change in the capacitance value significantly when $p/g > 0.5$. In Figure 5(b), the S-parameters are presented in terms of S_{11} and S_{12} for only Kodak photo paper.

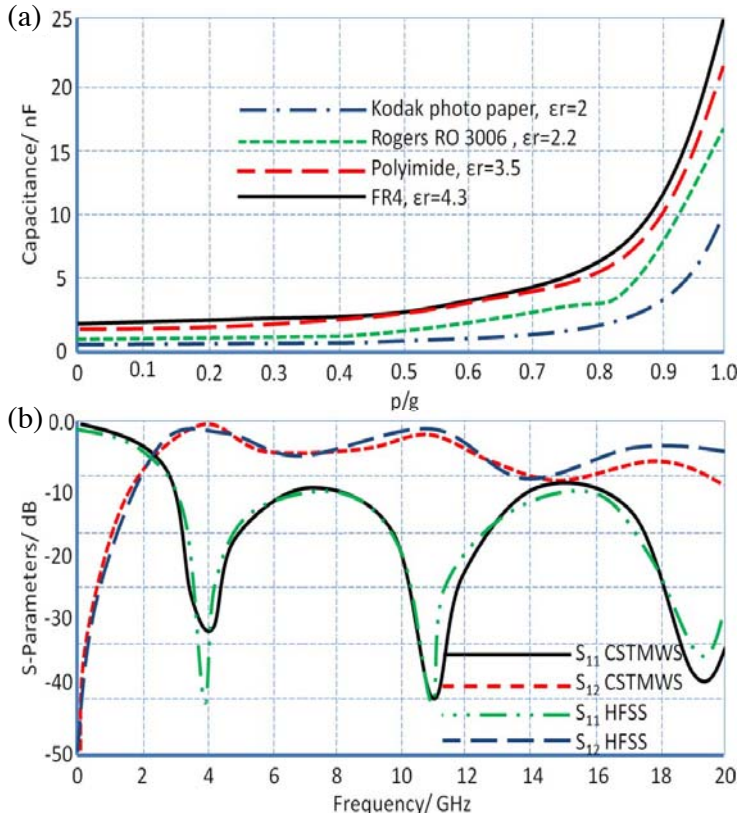

Figure 5. MTM characteristics based transmission line structure; (a) Capacitance and (b) S-parameters.

4. ANTENNA DESIGN DETAILS

The aim of the proposed design is to maximize the antenna bandwidth in which $|S_{11}| < -10$. Kodak photo paper of 0.5 mm thickness (h) and $\varepsilon_r = 2$ with $\tan\delta = 0.0015$ on area of 32 mm × 28 mm is considered for the antenna substrate. In the proposed design, a 50 Ω feed line is connected to a Vivaldi fractal patch printed on the Kodak substrate as seen in Figure 6. Indeed, the antenna design is started from an equilateral triangular patch; however, such a design provides narrow bandwidths around multiple frequency bands [6]. Therefore, a partial ground plane is proposed to provide a significant bandwidth enhancement by suppressing surface wave diffractions from the ground plane edges [12]. The proposed ECFCPW is developed to connect the SMA port to the patch continuously and maximize the matching bandwidth [18]. Flared matching circuits are introduced to enhance the

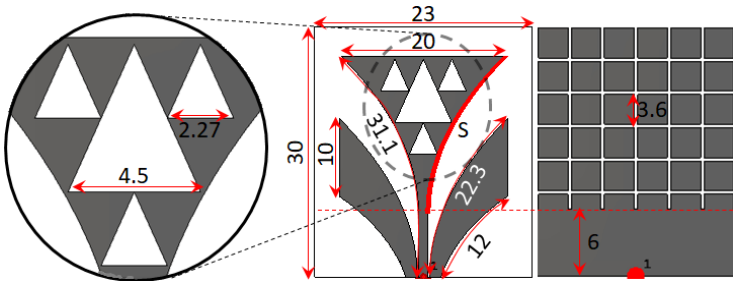

Figure 6. The proposed antenna structure based on the calculated dimensions. Note: The dimensions are in mm scale.

antenna bandwidth [4]. A further modification is considered in this design by including triangular slots on the patch to create new resonance modes by increasing surface current paths on the patch [16]. Then, the surface electrical area of the patch within the same physical area is increased. The proposed antenna is conducted to short plates to the proposed ECFCPW to work as matching circuits [12]. Finally, MTM-defects are introduced, see Figure 3, to the partial ground plane to improve the antenna matching with excellent enhancements in the antenna directivity, gain, and beamwidth due to suppressing the surface waves [3]. Therefore, it is worth to mention that the novelty of the proposed antenna design can be realized as a Vivaldi structure printed on the same side of the substrate. In fact, this ensures that the position of the MTM is not intersecting with the antenna operation. Nevertheless, the MTM layer could operate as a shielding layer to the human body when the antenna is mounted as a wearable device [10]. These MTM structures on the ground plane are defected as square *pads* to enhance the tangential component of the electric field and antenna radiation efficiency [9]. Also, it is good to mention that the Vivaldi antenna radiation pattern usually is highly directive which limits its use in RF harvesting application. Therefore, the originality of the proposed antenna is to have omnidirectional radiation from a Vivaldi design structure on top of the advantages of the traditional Vivaldi antenna.

The proposed antenna patch is constructed from a Sierpinski triangle fractal shape of the second order. The frequency resonance (f_r) of the proposed fractal can be derived from the following equations:

$$f_r = 0.26\frac{c}{h_e}2^n \tag{9}$$

$$h_e = \frac{\sqrt{3}}{2}\left[S + t\left(\varepsilon_r\right)^{-0.5}\right] \tag{10}$$

where c is the speed of light, S the side length of the patch, t the substrate thickness, and ε_r the substrate dielectric properties. Therefore, according to Equation (9), the proposed antenna must have the first frequency resonance at 2.34 GHz with a fractal index $n = 2$.

5. ANTENNA PERFORMANCE AND NUMERICAL RESULTS

5.1. Performance of the Planar Antenna Profile

The objective of this section is to study the antenna performance in terms of S_{11} and gain spectra using CSTMWS software package. The proposed antenna performance is tested numerically by changing the fractal index order from $n = 0$ to 2 to monitor the effects of that on the S_{11} spectra and gain characteristics. The antenna S_{11} spectrum is presented in Figure 7(a). It is found that the proposed antenna provides a bandwidth coverage from 3.1 GHz up to 20 GHz with excellent matching at $|S_{11}| < -10$ dB. The antenna provides a gain of 1.8 dBi at 3.1 GHz, which increases rapidly up to 4 dBi at 4 GHz compared to increases to 5 dBi in a graduate manner at 20 GHz as seen in Figure 7(b).

5.2. Exponential Factor Effects on the Antenna Performance

The effects of changing the factors a_1 and a_2 on the exponential functions of the ECFCPW matching circuits are investigated. This study is applied to realize the best values of a_1 and a_2 to obtain maximum matching bandwidth. Therefore, a parametric study is conducted by changing the values of a_1 and a_2 from 1 to 4 with according manner. As seen in Figure 8, the best matching can be obtained when a_1 is 2, and a_2 is 3. It should be mentioned that a_1 and a_2 are unit less values. It is noticed that the obtained values are found suitable enough for removing the imaginary parts to realize pure resistive load that enhances the matching [2].

5.3. Bending Effects on the Antenna Performance

In this section, the effect of bending is introduced as a part of this study to monitor the change in S_{11} and gain spectra. These parameters are evaluated numerically at the radius of bending of 10 cm, 9 cm, and 8 cm. In Figure 9(a), the evaluated S_{11} spectra are shown. It is found that antenna bending provides a positive change on the antenna bandwidth. Nevertheless, insignificant effect is found on the main antenna frequency bandwidth. Such a behavior is attributed to the fact of using the proposed

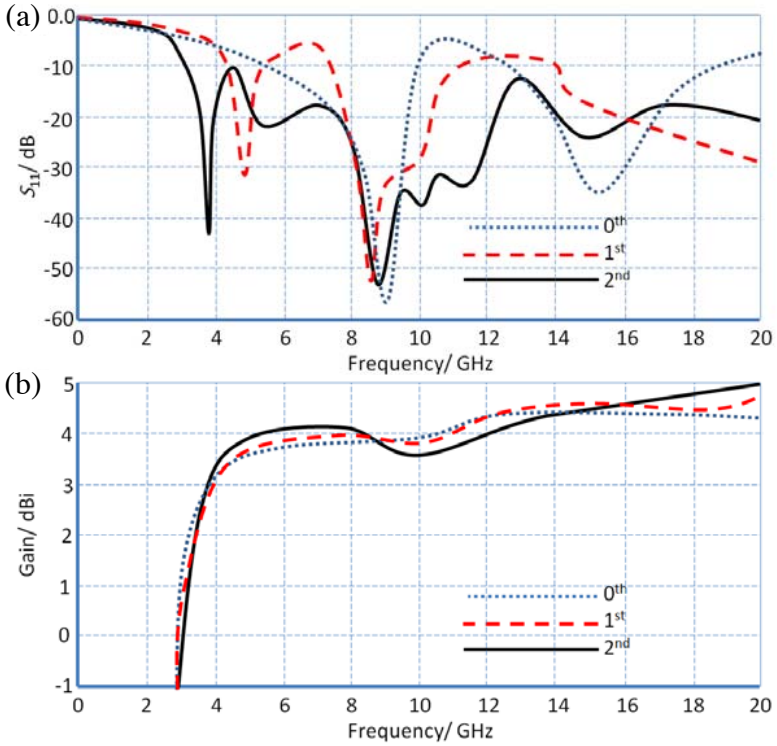

Figure 7. Simulated antenna properties: (a) S_{11} and (b) gain.

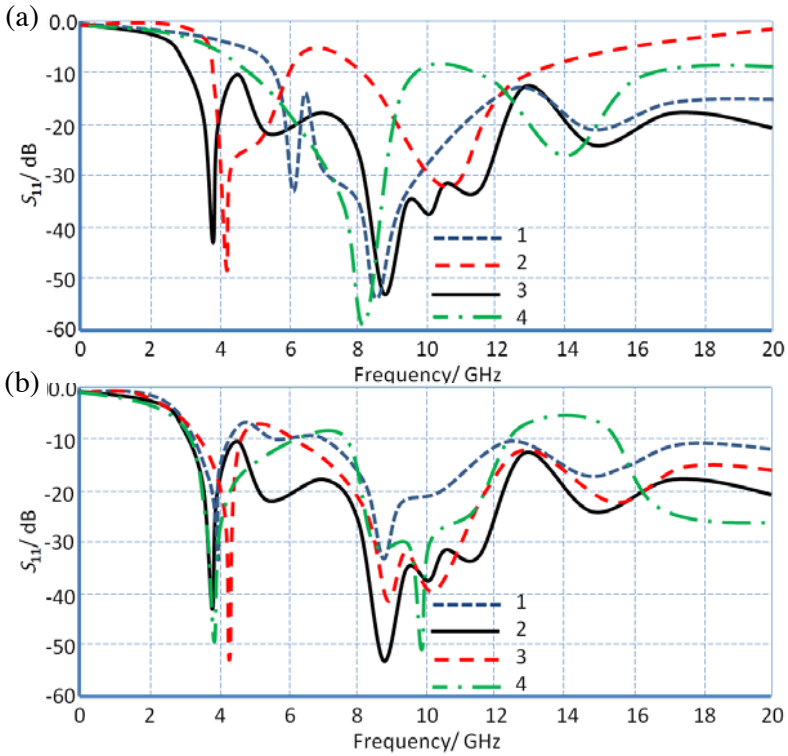

Figure 8. S_{11} spectra variation with respect to a_1 and a_2 values change; (a) with respect to a_1 change and (b) with respect to a_2 change.

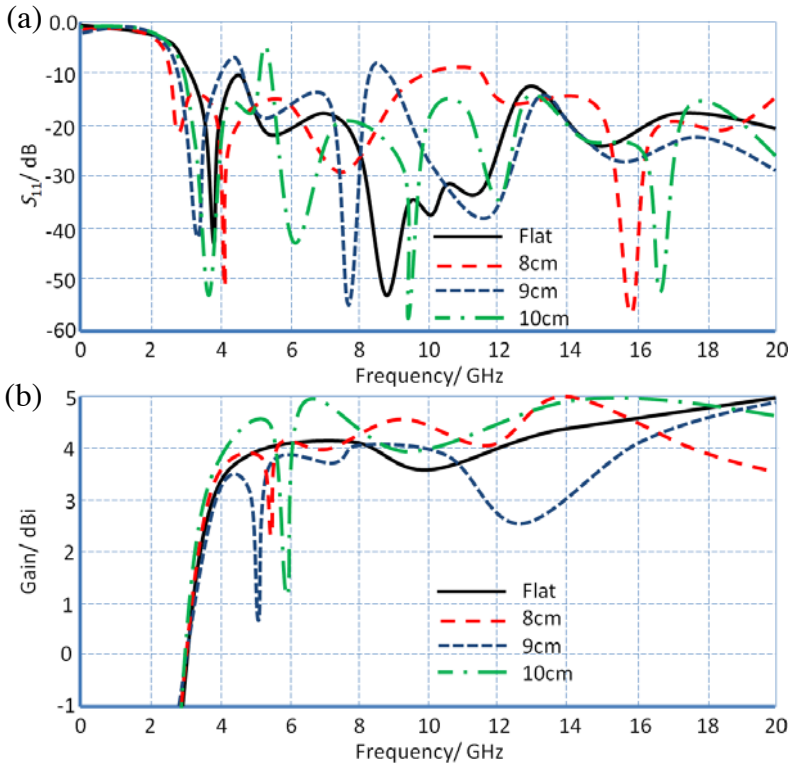

Figure 9. Antenna performance with different bending radii in comparison to the flat profile: (a) S_{11} spectra and (b) gain spectra.

feeding technique, in which, the resonance is completely affected by the width of the ground and the separation distance between the slots [9]. Nevertheless, the gain spectra are found to be mainly affected at a very narrow frequency band at each interval of bending as seen in Figure 9(b). This is due to the difficulty of the current motion at the frequency band between 5 GHz and 6 GHz, where the surface wave diffraction from the patch edges becomes significant [6]. Moreover, the electromagnetic aperture of the antenna depends on the slots location with respect to the antenna face center [5]. Also, it is important to mention that the proposed antenna shows excellent stability against bending in terms of gain because of the effects of the ground plane to keep the current distribution constant on the patch surface [1].

5.4. Antenna Efficiency

The antenna efficiency of the proposed antenna when it is considered as a rectenna is tested in this section. Therefore, the effects of changing the bending degree are characterized numerically by monitoring the efficiency. The relative results of such a study are presented in Figure 10. It is found that the proposed antenna shows a significant variation in the efficiency. This is due to bending effects that change the antenna surface impedance which realizes a change in the antenna matching [12].

6. ANTENNA FABRICATION AND EXPERIMENTAL MEASUREMENTS

6.1. Antenna Fabrication

A wideband antenna is generally fabricated by printing technology process based on inkjet material Fujifilm 2D printer machine [9]. The fabrication accuracy of such a technology is up to 6 µm printed trace [10]. The antenna structure, patch and ground, is printed on a photo paper from two sides. The fabricated prototype, front and back panels, is depicted in Figures 11(a) and (b).

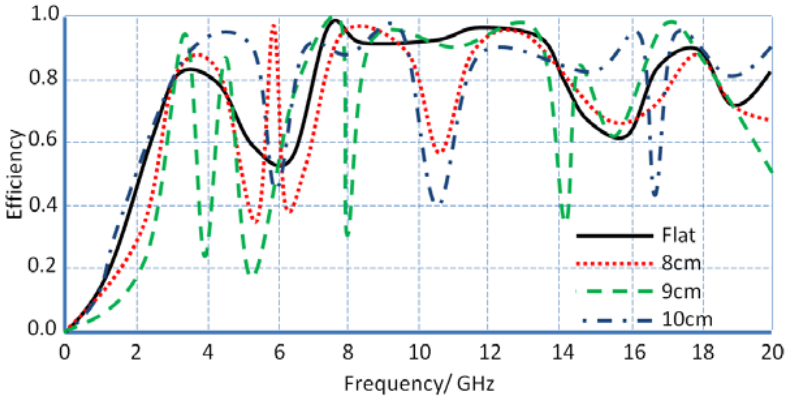

Figure 10. Antenna efficiency variation with changing the radius of bending.

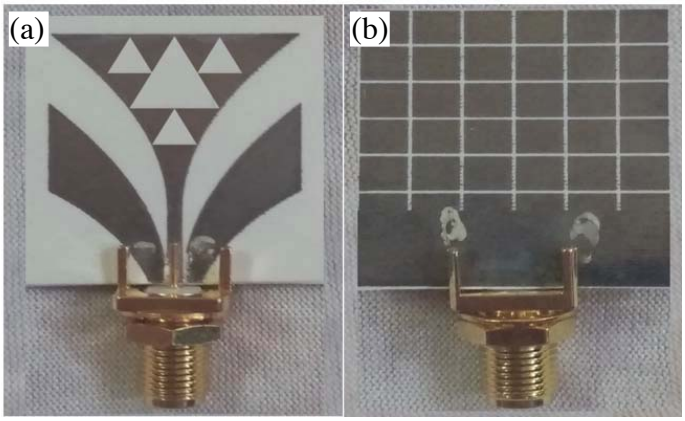

Figure 11. The fabricated antenna prototype: (a) Front view and (b) back view.

Table 1. The proposed antenna rectification performance in comparison to the published results.

References	Dimensions/mm^2	Freq./GHz	V_{DC}/V	Efficiency/%
[3]	261 × 5	2.45	0.20	30
[4]	90 × 160	5.8	0.23	30
[5]	100 × 70	2.45	1.12	74
[6]	500 × 500	1.60	0.15	8.5
[7]	120 × 40	5.8	0.03	44
[10]	100 × 100	2.45	2.13	82
[11]	70 × 70	0.91	0.35	55
This work	30 × 23	3.1	1.4	45
This work	30 × 23	4	1.3	42

6.2. Antenna Measurements

The performance in terms of S_{11} of the fabricated prototype is tested and measured then compared against the numerical simulations. The simulated results from CSTMWS are compared against the measurements. A good agreement between the simulated and measured results is achieved. Agilent N5230A Vector Network Analyzer (VNA) is invoked to perform the measurements. The measured S_{11}

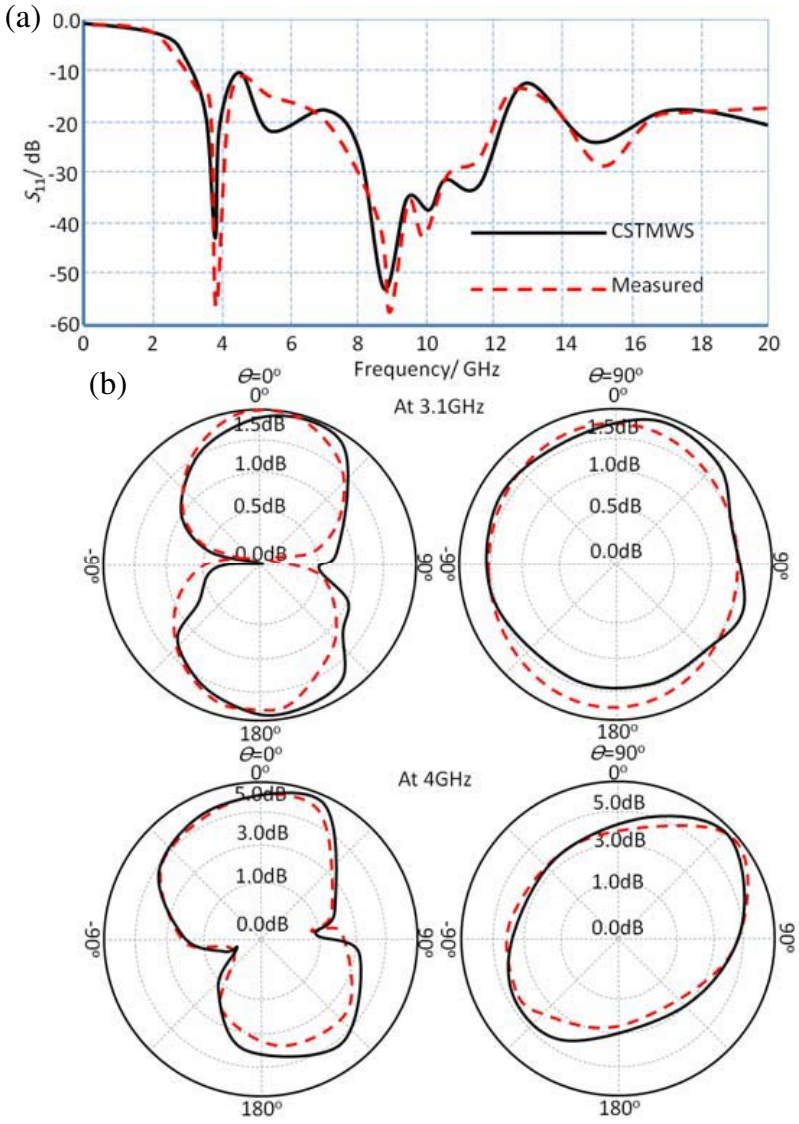

Figure 12. Comparison between measured and simulated results; (a) S_{11} spectra and (b) far-field radiation patterns at 3.1 GHz and 4 GHz.

spectrum shows excellent agreement with the simulated results as shown Figure 12(a). The measured far-field radiation patterns at E and H-planes are presented in Figure 12(b) for 3.1 GHz and 4 GHz.

6.3. Rectenna Performance

The rectification efficiency of the proposed antenna is tested by connecting the proposed antenna to a wireless energy harvesting commercial module card of RFD102A series. It is found that the proposed rectifying antenna shows an output voltage of 1.4 V at 3.1 GHz and 1.3 V at 4 GHz. The rectification efficiency is found to be increased gradually up to 45% at 3.1 GHz when the transmitted power is 8 dBm as seen in Figure 13(a). Nevertheless, the antenna shows about 42% rectification efficiency at 4 GHz as depicted in Figure 13(b).

The proposed antenna performances in terms of output voltage and antenna size and performance are compared to other published results. It is found that the proposed antenna performances show a significant advancement in comparison to the recent published work as listed in Table 1.

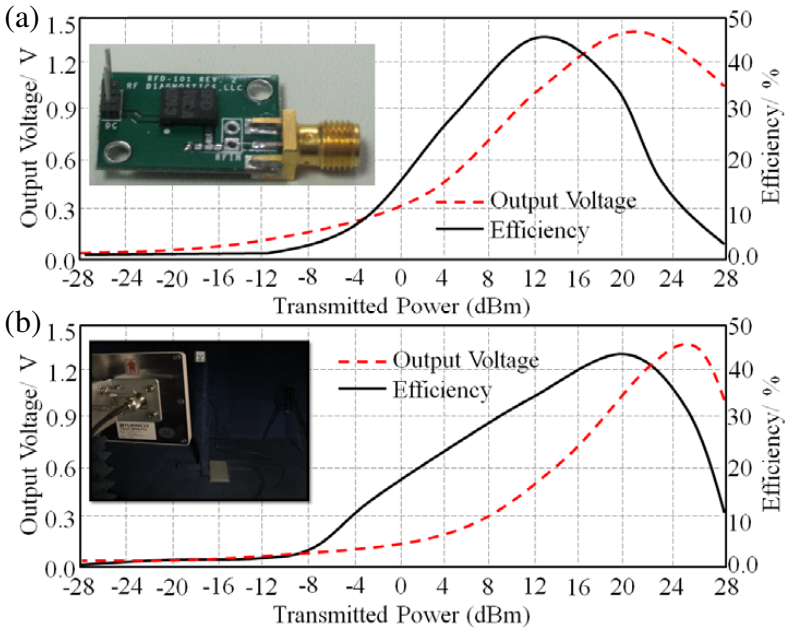

Figure 13. Measured rectification performance at; (a) 3.1 GHz and (b) 4 GHz.

7. CONCLUSION

This paper intensively investigates, based on an analytical and numerical studies supported by experimental validations, the possibility of using a UWB Vivaldi fractal antenna for RF energy harvesting. The proposed antenna is constructed from a microstrip patch with Sierpinski triangle fractal slots. The patch structure is fed with a flared CPW with a flared matching circuit for antenna bandwidth enhancement. The antenna ground plane is proposed as a partial continues layer defected with MTM pads to enhance the antenna radiation efficiency. The proposed antenna is tested when being connected to a full wave bridge rectifier board for RF harvesting. Therefore, the harvesting efficiency is found about 45% at 3.1 GHz and 42% at 4 GHz. Nevertheless, the obtained harvested output voltage is found about 1.4 V and 1.3 V at 3.1 GHz and 4 GHz, respectively.

REFERENCES

1. Al-Sabbagh, H. M., T. A. Elwi, Y. Al-Naiemy, and H. M. Al-Rizzo, "A compact triple-band metamaterial-inspired antenna for wearable applications," *Microwave and Optical Technology Letters*, Vol. 62, 763–777, October 2019.
2. Pozar, D. M., *Microwave Engineering*, 3rd edition, Chapter 5, Wiley, Hoboken, NJ, 2012.
3. Elwi, T. A., "A further realization of a flexible metamaterial-based antenna on nickel oxide polymerized palm fiber substrates for RF energy harvesting," *Wireless Personal Communications*, Vol. 10, No. 12, 1–15, August 2020.
4. Shen, S., C. Y. Chiu, and R. D. Murch, "A broadband L-probe microstrip patch rectenna for ambient RF energy harvesting," *2017 IEEE International Symposium on Antennas and Propagation USNC/URSI National Radio Science Meeting*, 2037–2038, July 2017.
5. Elwi, T. A., "Further investigation on solant-rectenna based flexible Hilbert-shaped metamaterials," *IET Nanodielectrics*, Vol. 4, No. 12, 1–12, March 2020.
6. Shen, S., C. Y. Chiu, and R. D. Murch, "Multiport pixel rectenna for ambient RF energy harvesting," *IEEE Trans. Antennas Propag.*, Vol. 66, No. 2, 644–656, February 2018.

7. Shen, S., C. Y. Chiu, and R. D. Murch, "A dual-port triple-band L-probe microstrip patch rectenna for ambient RF energy harvesting," *IEEE Antennas Wireless Propag. Lett.*, Vol. 16, 3071–3074, 2017.
8. Elwi, T. A., "Remotely controlled reconfigurable antenna for modern applications," *Microwave and Optical Technology Letters*, Vol. 6, No. 1, 1–19, April 2020.
9. Elwi, T. A., M. A. Rasheed, L. W. Anber, and M. Q. Fahad, "Gain enhancement of a miniaturized inverted λ-dipole antenna," *IEEE ICICT19 International Conference for Information and Communication Technology*, April 2019.
10. Olgun, U., C.-C. Chen, and J. L. Volakis, "Investigation of rectenna arrayconfigurations for enhanced RF power harvesting," *IEEE Antennas Wireless Propag. Lett.*, Vol. 10, 262–265, 2011.
11. Hagerty, J. A., F. B. Helmbrecht, W. H. McCalpin, R. Zane, and Z. B. Popovic, "Recycling ambient microwave energy with broad-band rectenna arrays," *IEEE Trans. Microw. Theory Techn.*, Vol. 52, No. 3, 1014–1024, March 2004.
12. Almoneef, T. S., H. Sun, and O. M. Ramahi, "A 3-D folded dipole antenna array for far-field electromagnetic energy transfer," *IEEE Antennas Wireless Propag. Lett.*, Vol. 15, 1406–1409, 2016.
13. Shen, S. and R. D. Murch, "Impedance matching for compact multiple antenna systems in random RF fields," *IEEE Trans. Antennas Propag.*, Vol. 64, No. 2, 820–825, February 2016.
14. Shen, S., Y. Sun, S. Song, D. P. Palomar, and R. D. Murch, "Successive Boolean optimization of planar pixel antennas," *IEEE Trans. Antennas Propag.*, Vol. 65, No. 2, 920–925, February 2017.
15. Azeez, A. R., T. A. Elwi, and Z. A. Abed AL-Hussain, "A numerical study of the antipodal Vivaldi antenna design for ultrawideband applications," *SAUSSUREA Multidisciplinary International Peer Reviewed Journal*, Vol. 6, No. 5, 366–370, August 2016.
16. Elwi, T. A., A. I. Imran, and Y. Alnaiemy, "A miniaturized Lotus Shaped microstrip antenna loaded with MTM structures for high gain-bandwidth product applications," *Progress In Electromagnetics Research C*, Vol. 60, 157–167, 2015.
17. Elwi, T. A., M. M. Hamed, Z. Abbas, and M. A. Elwi, "On the performance of the 2D planar metamaterial structure," *International Journal of Electronics and Communications*, Vol. 68, No. 9, 846–850, September 2014.
18. Elwi, T. A., S. Al-Frieh, M. Al-Bawi, and M. Noori, "No frequency reuse: Wearable steerable MIMO microstrip antenna array for wearable ad hoc applications," *British Journal of Applied Science & Technology*, Vol. 4, No. 17, 2477–2488, April 2014.
19. Elwi, T. A., M. Noori, Y. Al-Naiemy, and E. S. Yahiea, "Conformal antenna array for MIMO applications," *Journal of Electromagnetic Analysis and Applications*, Vol. 6, 43–50, March 2014.
20. Elwi, T. A., H. M. Al-Rizzo, D. G. Rucker, and H. R. Khaleel, "Effects of twisting and bending on the performance of a miniaturized truncated sinusoidal printed circuit antenna for wearable biomedical telemetry devices," *AEU-International Journal of Electronics and Communications*, Vol. 13, No. 1, 1–12, March 2010.
21. Elwi, T. A., "Metamaterial based a printed monopole antenna for sensing applications," *International Journal of RF and Microwave Computer-Aided Engineering*, August 2018.
22. Ahmed, H. S. and T. A. Elwi, "SAR effects reduction using reject band filter arrays for Wi-Fi portable devices," *International Journal of Electronics Letters*, Vol. 7, No. 2, 236–248, Taylor & Francis, May 2018.
23. Yang, F. and Y. R. Samii, *Electromagnetic Band Gap Structures in Antenna Engineering*, Cambridge University Press, 2009.
24. Elwi, T. A., "A slotted lotus shaped microstrip antenna based an MTM structure," *Journal of Material Sciences & Engineering*, Vol. 7, No. 2, March 2018.
25. www.cst.com.